

# Dynamical detection of extended nonergodic states in many-body quantum systems

David A. Zarate-Herrada,<sup>1</sup> Isaías Vallejo-Fabila,<sup>2</sup> Lea F. Santos,<sup>2</sup> and E. Jonathan Torres-Herrera<sup>1</sup>

<sup>1</sup>*Institute of Physics, Benemérita Universidad Autónoma de Puebla, 72570 Puebla, Pue., Mexico*

<sup>2</sup>*Department of Physics, University of Connecticut, Storrs, Connecticut 06269, USA*

Fractal dimensions are tools for probing the structure of quantum states and identifying whether they are localized or delocalized in a given basis. These quantities are commonly extracted through finite-size scaling, which limits the analysis to relatively small system sizes. In this work, we demonstrate that the correlation fractal dimension  $D_2$  can be directly obtained from the long-time dynamics of interacting many-body quantum systems. Specifically, we show that it coincides with the exponent of the power-law decay of the time-averaged survival probability, defined as the fidelity between an initial state and its time-evolved counterpart. This dynamical approach avoids the need for scaling procedures and enables access to larger systems than those typically reachable via exact diagonalization. We test the method on various random matrix ensembles, including full random matrices, the Rosenzweig-Porter model, and power-law banded random matrices, and extend the analysis to interacting many-body systems described by the one-dimensional Aubry-André model and the disordered spin-1/2 Heisenberg chain. In the case of full random matrices, we also derive an analytical expression for the entire evolution of the time-averaged survival probability.

## I. INTRODUCTION

Fractal dimensions are tools for probing scaling behavior near quantum phase transitions and for quantifying the complexity of quantum systems [1–41]. They provide insight into the structural properties of quantum states, enabling the distinction between localized and extended phases in both noninteracting [1–18] and interacting quantum models [19–31], and revealing universal features at critical points [11, 42–47]. Fractal dimensions also offer a means to explore the Hilbert space accessed under time evolution, providing information about quantum dynamics [19, 23–26, 28, 37, 48–51].

The focus of this work is the correlation fractal dimension  $D_2$ , which has had a predominant role in studies of localization and multifractality. As any fractal dimension,  $D_2$  is rigorously defined in the thermodynamic limit. However, since numerical studies are restricted to finite systems,  $D_2$  is extracted from scaling analyses of the inverse participation ratio (IPR) [52], requiring access to many different system sizes and full exact diagonalization. This procedure is computationally demanding, particularly when dealing with many-body quantum systems, because their Hilbert space dimension grows exponentially with system size. This makes it challenging to reliably obtain  $D_2$ , especially in the vicinity of critical points, where fluctuations are strong and convergence is slow [23].

We explore an alternative and efficient method for extracting the fractal dimension  $D_2$ , circumventing the limitations of scaling analyses. Instead of relying on the direct analysis of the structures of the eigenstates, we obtain  $D_2$  dynamically from the time-averaged survival probability, that is, the time-averaged fidelity between an initial state and its time-evolved counterpart [4–7, 53–55]. The power-law exponent governing the long-time decay of the time-averaged survival probability coincides with the fractal dimension  $D_2$ . This dynamical approach gives access to larger system sizes than those achieved via

exact diagonalization, thanks to advanced algorithms developed for simulating quantum dynamics [56–60].

An additional advantage of extracting  $D_2$  from dynamics is that the basis is unambiguously defined, corresponding to the energy eigenbasis. In contrast, usual calculations of fractal dimensions based on the IPR of eigenstates depend on the choice of basis, such as real space or momentum space. Nevertheless, the results of both the eigenstate-based and dynamical approaches depend on the energy window considered. Initial states are selected with energies close to the center of the spectrum, where many-body eigenstates typically exhibit the maximal degree of delocalization permitted by the system's regime. Furthermore, averaging over many initial states and disorder realizations reduces fluctuations and potential biases associated with specific state choices.

We compare four quantities: the power-law exponent governing the decay of the survival probability, the power-law exponent of the time-averaged survival probability decay, the fractal dimension  $D_2^{\text{IPR}_0}$  obtained from the scaling analysis of the  $\text{IPR}_0$  of the initial state in the energy eigenbasis [9, 10, 19, 61], and the fractal dimension  $D_2^{\text{box}}$  extracted from a box counting method [3, 4, 8, 11, 62–65]. We show that the survival probability is not only sensitive to the properties of the eigenstates, but it is also influenced by both spectral and system boundaries. In contrast, the time-averaged survival probability filters out spectral details and reflects only correlations among the components of quantum states, making it an appropriate quantity for extracting the fractal dimension from dynamics. We also find that the power-law exponent of the time-averaged survival probability shows closer agreement with  $D_2^{\text{box}}$  than with  $D_2^{\text{IPR}_0}$ , particularly near critical points.

The comparison between the power-law exponent  $\nu$  of the time-averaged survival probability decay and  $D_2^{\text{box}}$  has been previously explored in noninteracting models, such as the Aubry-André (Harper) model with a single excitation and quasiperiodic disorder [4, 7] and Fibonacci

models [4, 6], where the eigenstates are multifractal despite the absence of disorder. Our focus is instead on interacting systems, where the analyses of the structure of the eigenstates typically focus on  $D_2$  obtained from IPR, with some studies including the power-law exponent  $\gamma$  of the survival probability decay [19, 51, 66]. We examine all four quantities ( $D_2^{\text{IPR}_0}$ ,  $D_2^{\text{box}}$ ,  $\gamma$ , and  $\nu$ ) in both the random matrix models and the interacting systems, and find excellent agreement between  $\nu$  and  $D_2^{\text{box}}$  in all cases.

Building on the analytical derivation of the entire time evolution of the survival probability under full random matrices [21, 67, 68], we also derive an analytical expression for the time-averaged survival probability. The survival probability under full random matrices of the Gaussian orthogonal ensemble (GOE) [69] decays with a power-law exponent  $\gamma = 3$ , which does not match the fractal dimension, since  $0 \leq D_2 \leq 1$ . In contrast, the time-averaged survival probability decays with an exponent  $\nu = 1$ , consistent with the fractal dimension of eigenstates are maximally delocalized as in full random matrices. This demonstrates our claim that the time-averaged survival probability suppresses the influence of spectral properties and captures correlations among the components of a quantum state, making it the most suitable dynamical quantity for extracting the fractal dimension.

The structure of the paper is as follows. In Sec. II, we introduce the relevant observables and present the two ways to obtain the fractal dimension  $D_2$ , based on the IPR and on the box-counting method. In Sec. III, we benchmark our approach on random matrix ensembles, using first matrices from the GOE, and then ensembles of random matrices that exhibit a localization-delocalization transition, namely the Rosenzweig-Porter (RP) model [70–74] and the power-law banded random matrix (PBRM) model [32–34, 39, 41, 75–80]. In Sec. IV, we extend our analysis to two many-body quantum systems: the Aubry-André model with interactions [81, 82], and the disordered Heisenberg spin-1/2 chain [29, 83–85].

## II. SURVIVAL PROBABILITY AND FRACTAL DIMENSION

This section introduces the quantities analyzed in this work. On the dynamical side, we focus on the survival probability and the time-averaged survival probability. To directly probe the structure of the eigenstates, we compute the fractal dimension  $D_2$  using two approaches: the box-size scaling method and the scaling analysis of the IPR.

### A. Survival Probability

The survival probability gives the probability of finding the system in the initial state  $|\Psi(0)\rangle$  at time  $t$ . Mathematically it is given by,

atically it is given by,

$$S_P(t) = |\langle \Psi(0) | \Psi(t) \rangle|^2 = \left| \sum_{n=1}^N |C_n^{(0)}|^2 e^{-iE_n t} \right|^2 \quad (1)$$

$$= \sum_{n \neq m}^N |C_n^{(0)}|^2 |C_m^{(0)}|^2 e^{-i(E_n - E_m)t} + \text{IPR}_0,$$

where  $C_n^{(0)} = \langle \psi_n | \Psi(0) \rangle$  are the coefficients of the initial state projected in the energy eigenbasis  $\{|\psi_n\rangle\}$  of the system's Hamiltonian,  $H|\psi_n\rangle = E_n|\psi_n\rangle$ ,  $N$  is the dimension of the Hilbert space, and  $\text{IPR}_0$  is the saturation value of  $S_P(t)$  in the absence of too many degeneracies. This asymptotic value corresponds to the IPR of the initial state in the energy eigenbasis,

$$\text{IPR}_0 = \sum_{n=1}^N |C_n^{(0)}|^4. \quad (2)$$

At very short times, the survival probability shows a universal quadratic behavior followed by dynamical features that depend on the model and initial state [86, 87]. At intermediate times, the survival probability averaged over initial states and disorder realizations often exhibits a power-law decay

$$\langle S_P(t) \rangle \propto t^{-\gamma}. \quad (3)$$

In the equation above,  $\langle \cdot \rangle$  indicates average and the exponent  $\gamma$  carries information about the components of the eigenstates [19, 88–91] and the bounds of the spectrum [89, 90, 92–94].

The time-averaged survival probability

$$\overline{\langle S_P(t) \rangle} = \frac{1}{t} \int_0^t \langle S_P(\tau) \rangle d\tau, \quad (4)$$

reduces the temporal fluctuations present in  $S_P(t)$  and also exhibits a power-law decay,

$$\overline{\langle S_P(t) \rangle} \propto t^{-\nu}, \quad (5)$$

where  $\nu$  does not necessarily coincide with  $\gamma$  in Eq. (3). In this work, we compare  $\gamma$  and  $\nu$  with the fractal dimension  $D_2$ .

For the time evolution, a total number of  $10^4$  samples of initial states and disorder realizations are used for the averages. The initial states are selected so that their energies,  $\langle \Psi(0) | H | \Psi(0) \rangle$ , lie near the center of the spectrum.

### B. Fractal Dimension

The value of the fractal dimension  $D_2$  has information about the structure of a quantum state. The state is fully delocalized (ergodic) when  $D_2 = 1$ , extended but nonergodic when  $0 < D_2 < 1$ , and localized if  $D_2 = 0$ .

We describe below two common approaches to extract  $D_2$ .

(i) One method is based on the scaling analysis of the  $\text{IPR}_0$  [Eq. 2] with respect to the Hilbert space dimension  $N$  [12, 34, 95–97], since

$$\text{IPR}_0 \propto N^{-D_2^{\text{IPR}_0}}. \quad (6)$$

The analysis is performed by plotting the average  $\langle \ln(\text{IPR}_0) \rangle$  versus  $\ln N$ , where the negative slope gives an estimate of  $D_2^{\text{IPR}_0}$ . Using  $\langle \ln(\text{IPR}_0) \rangle$  instead of  $\ln(\text{IPR}_0)$  reduces statistical fluctuations more effectively. While some studies analyze the scaling of the IPR for eigenstates in a fixed basis, we find that this approach can lead to significant deviations from  $\nu$ , especially near critical regions. Overall,  $\nu$  and quantities that agree with it are more sensitive to multifractality than  $D_2$  obtained from eigenstates.

(ii) The other approach to the fractal dimension  $D_2$  is the box-counting method [3–7, 11, 62–65]. It consists of dividing the spectrum into boxes  $B_i$  of size  $l$  and computing the probability  $\sum_{E_n \in B_i} |C_n^{(0)}|^2$ , which is obtained with the components of the initial state corresponding to the eigenstates with energy  $E_n$  in  $B_i$ . The total probability is the sum over the total number  $N_B(l)$  of boxes of size  $0 < l \leq 1$ ,

$$P(l) = \sum_{i=1}^{N_B(l)} \left( \sum_{E_n \in B_i} |C_n^{(0)}|^2 \right)^2. \quad (7)$$

The fractal dimension  $D_2^{\text{box}}$  is extracted from scaling with respect to the box size  $l$ ,

$$P(l) \propto l^{D_2^{\text{box}}}. \quad (8)$$

Above,  $P(l)$  is the probability that the difference between the energies of any two eigenstates from the spectral decomposition of  $|\Psi(0)\rangle$  is less than  $l$ . We calculate  $P(l)$  by normalizing the spectrum length to  $l = 1$ , so that a box of size  $l = 1$  includes all components  $|C_n^{(0)}|^2$  and  $P(1) = 1$ . The scaling analysis is performed for  $l \ll 1$ .

The fractal dimension  $D_2^{\text{box}}$  probes the distribution of the components of  $|\Psi(0)\rangle$  in energy at different scales  $l$ , being a more local measure than  $D_2^{\text{IPR}}$ . While  $D_2^{\text{box}}$  can, in principle, be computed for even a single state,  $D_2^{\text{IPR}}$  often uses ensemble averages. Furthermore,  $D_2^{\text{box}}$  is directly related to the exponent of the power-law decay of  $\langle S_P(t) \rangle$  [4].

In this work, the results for  $D_2^{\text{IPR}_0}$  obtained from scaling analyses are based on averages over disorder realizations and initial states. All averages consider  $10^4$  samples, as in the analysis for the power-law exponents.

### III. RANDOM MATRICES

This section compares the power-law decay exponents of  $\langle S_P(t) \rangle$  and  $\overline{\langle S_P(t) \rangle}$  with  $D_2^{\text{IPR}_0}$  and  $D_2^{\text{box}}$  for the GOE, RP, and PBRM models.

#### A. GOE matrices

The GOE consists of real and symmetric  $N \times N$  matrices completely filled with random numbers from a Gaussian distribution with mean zero and variance given by

$$\langle H_{ij}^2 \rangle = \begin{cases} 1/2, & \text{for } i \neq j, \\ 1, & \text{for } i = j. \end{cases} \quad (9)$$

The eigenvalues of these matrices are highly correlated [69] and the eigenstates are normalized random vectors.

We consider initial states corresponding to the diagonal part of the random matrix. Since the eigenstates are normalized random vectors, the components of these initial state,  $C_n^{(0)}$ , are random numbers from a Gaussian distribution with  $\langle C_n^{(0)} \rangle \sim 0$ ,  $\langle C_n^{(0)} \rangle^2 \sim 1/N$ , and  $\langle C_n^{(0)} \rangle^4 \sim 3/N^2$ , so  $\langle \text{IPR}_0 \rangle \sim 3/N$  and  $D_2^{\text{IPR}_0} \sim 1$ .

Similarly, the box-counting method gives  $D_2^{\text{box}} \sim 1$ , since for GOE matrices, we have approximately  $lN$  eigenstates with energy  $E_n$  in a box of size  $l$ . This implies that  $\sum_{E_n \in B_i} |C_n^{(0)}|^2 \sim l$  and  $P(l) \sim l$ .

Using GOE matrices, it is possible to derive an analytical expression for the survival probability [21, 68]

$$\langle S_P(t) \rangle = \frac{1 - \overline{S_P}}{N - 1} \left[ N \frac{\mathcal{J}_1^2(2\Gamma t)}{(\Gamma t)^2} - b_2 \left( \frac{\Gamma t}{2N} \right) \right] + \overline{S_P}, \quad (10)$$

where  $\Gamma = \sqrt{N/2}$  is the width of the energy distribution of the initial state,  $\mathcal{J}_1$  is the Bessel function of first kind,  $\overline{S_P} = 3/(N + 2)$  [98, 99] and  $b_2(t)$  is the two-level form factor,

$$b_2(t) = \Theta(1 - t)[1 - 2t + t \ln(2t + 1)] + \Theta(t - 1)\{t \ln[(2t + 1)/(2t - 1)] - 1\} \quad (11)$$

where  $\Theta(t)$  is the Heaviside step function. The first term in Eq. (10), involving the Bessel function, controls the short- and intermediate-time decay of the survival probability, the second term, with the  $b_2(t)$  function, governs the long-time behavior up to the saturation at  $\overline{S_P}$ .

Figure 1 compares the analytical expression in Eq. (10) (light blue line) with the corresponding numerical result (dark blue line). The oscillations observed in both curves originate from the term with the Bessel function in the analytical expression and exhibit a power-law decay  $\propto t^{-3}$ . The Bessel function arises from the square of the Fourier transform of the energy distribution of the initial state, which follows a semicircular form [86]. The power-law exponent  $\gamma = 3$  is a consequence of the sharp edges of the semicircular energy distribution, being clearly unrelated with the fractal dimension  $D_2^{\text{IPR}_0} = 1$ . The exponent  $\gamma = 3$  reflects spectral properties rather than the structure of the eigenstates.

At long times,  $\langle S_P(t) \rangle$  shows a dip below the saturation value known as the correlation hole [98, 100–102]. It is characterized by the  $b_2(t)$  function and emerges only in systems with level repulsion.

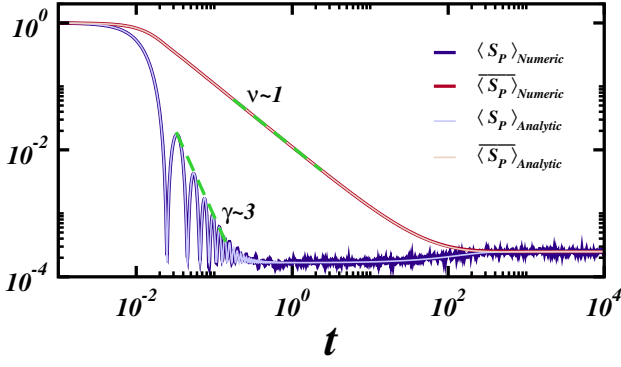


FIG. 1. Analytical expression for the survival probability  $\langle S_P(t) \rangle$  in Eq. (10) (light blue), numerical results (dark blue), analytical expression for the time-averaged survival probability  $\overline{\langle S_P(t) \rangle}$  in Eq. (12) (dark red), and numerical results (light red) for matrices from the GOE;  $N = 12\,000$ .

The decay behavior of the survival probability changes when time averaging is introduced. For the time-averaged survival probability  $\overline{\langle S_P(t) \rangle}$ , the power-law decay exponent becomes  $\nu = 1$  in contrast to the faster decay of the survival probability. By performing the integration in Eq. (4) (see Appendix A), we obtain the analytical expression

$$\overline{\langle S_P(t) \rangle} = \frac{\overline{S_P}}{3} \left[ 4N\mathcal{I}_1(2\Gamma t) - \mathcal{I}_2\left(\frac{\Gamma t}{2N}\right) \right] + \overline{S_P}. \quad (12)$$

For times,  $\Gamma t \gg 1$ , we reach the asymptotic results

$$\mathcal{I}_1(2\Gamma t) \approx \frac{2}{3\pi\Gamma t} + O(t^{-2}), \quad (13)$$

$$\mathcal{I}_2\left(\frac{\Gamma t}{2N}\right) \approx \frac{N}{2\Gamma t} + O(t^{-2}), \quad (14)$$

leading to the large-time behavior

$$\overline{\langle S_P(t \rightarrow \infty) \rangle} \approx \frac{8}{9\pi} \frac{N}{\Gamma t} \overline{S_P} - \frac{1}{6} \frac{N}{\Gamma t} \overline{S_P} + \overline{S_P} + O(t^{-2}). \quad (15)$$

This result confirms that  $\overline{\langle S_P(t) \rangle} \propto t^{-1}$ . The absence of Bessel-function-induced oscillations reflects the fact that information about the spectrum has been averaged out. The decay of the time-averaged survival probability is governed by the structure of the initial states and the power-law decay exponent  $\nu$  agrees with the fractal dimension  $D_2^{\text{box}}$ . When the components of the initial states and of the eigenstates are uncorrelated random variables,  $\nu = D_2^{\text{box}} = D_2^{\text{IPR}_0} = 1$ .

Figure 1 shows that the analytical result for the time-averaged survival probability in Eq. (12) (dark red line) is in excellent agreement with the numerical result (light red line). The power-law decay persists up to saturation, with no indication of a correlation hole, and the exponent  $\nu = 1$  coincides with the fractal dimension.

## B. Rosenzweig-Porter matrices

The RP model was introduced in the context of nuclear physics [70] to study the transition between regular and chaotic spectra in complex nuclei. The ensemble consists of random matrices with entries taken from a Gaussian distribution with mean zero and variance

$$\langle H_{ij}^2 \rangle = \begin{cases} 1, & i = j \\ \frac{1}{2}N^{-\alpha}, & i \neq j, \end{cases} \quad (16)$$

where  $N$  is the dimension of the matrix and  $\alpha$  is the control parameter. The ensemble presents different phases depending on the value of  $\alpha$ : an ergodic phase when  $\alpha < 1$ , a nonergodic extended phase with extended nonergodic states when  $1 < \alpha < 2$ , and a localized phase for  $\alpha > 2$  [73, 103–105]. We recover the GOE when  $\alpha = 0$  and a diagonal random matrix is obtained for  $\alpha \rightarrow \infty$ .

We begin by comparing the power-law exponents  $\gamma$  and  $\nu$  obtained from the decay of the survival probability  $\langle S_P(t) \rangle$  and the time-averaged survival probability  $\overline{\langle S_P(t) \rangle}$ , respectively, across different values of  $\alpha$ . Next, we illustrate the procedure for computing the fractal dimensions  $D_2^{\text{IPR}_0}$  and  $D_2^{\text{box}}$  through explicit examples. Finally, we compare all relevant quantities:  $\gamma$ ,  $\nu$ ,  $D_2^{\text{IPR}_0}$ , and  $D_2^{\text{box}}$ . Our analysis shows that  $\nu$  from  $\overline{\langle S_P(t) \rangle}$  and  $D_2^{\text{box}}$  are in agreement and offer the most reliable indicators for identifying the system's regime, whether delocalized, critical, or localized.

In Fig. 2(a), where  $\alpha = 0.1$ , the behaviors of  $\langle S_P(t) \rangle$  and  $\overline{\langle S_P(t) \rangle}$  are similar to those for the GOE in Fig. 1, with  $\gamma > D_2^{\text{IPR}_0} \sim 1$  for  $\langle S_P(t) \rangle$  and  $\nu = D_2^{\text{box}} \sim 1$  for  $\overline{\langle S_P(t) \rangle}$ . As  $\alpha$  increases from the delocalized regime [Fig. 2(a)] to the localized regime in Fig. 2(d), both power-law exponents decrease, with  $\gamma$  remaining larger than  $\nu$  throughout. The behavior of  $\langle S_P(t) \rangle$  changes significantly from the delocalized [Fig. 2(a)] to the intermediate regime [Fig. 2(c)]. In the first case,  $\langle S_P(t) \rangle$  exhibits oscillations during its power-law decay and a later correlation hole, while in the intermediate regime, the oscillations vanish and the correlation hole gradually disappears.

In Fig. 3, we illustrate how the fractal dimension is obtained from the IPR [Fig. 3(a)] and from the box-counting method [Fig. 3(b)] for some values of the control parameter  $\alpha$ . In Fig. 3(a), we fit the data for  $\langle \ln(\text{IPR}_0) \rangle$  vs  $\ln N$  with a straight line, and the slope corresponds to  $D_2^{\text{IPR}_0}$ . In Fig. 3(b), the curves for  $P(l)$  are nearly flat for small  $l$  and they saturate for large  $l$ . We obtain  $D_2^{\text{box}}$  from the interval of the log-log plot where the curves are linear.

Figure 4 compares all four quantities:  $\gamma$ ,  $\nu$ ,  $D_2^{\text{IPR}_0}$ , and  $D_2^{\text{box}}$ . There is excellent agreement between the exponent  $\nu$  of the time-average survival probability and  $D_2^{\text{box}}$  for all values of  $\alpha$ . The exponent  $\nu$  and the fractal dimension  $D_2^{\text{box}}$  also align well with  $D_2^{\text{IPR}_0}$  in the ergodic and localized regimes, but not so well in the extended nonergodic

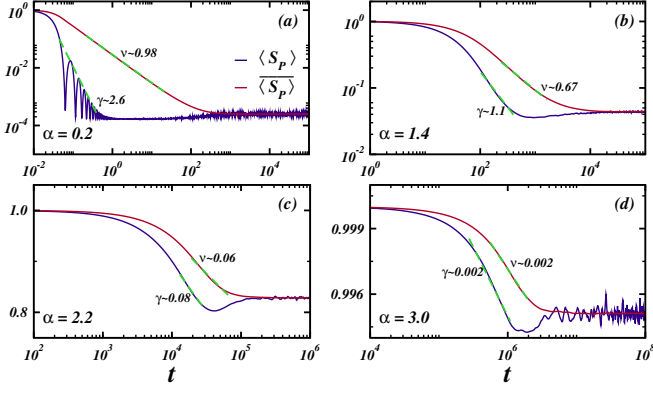


FIG. 2. Survival probability  $\langle S_P(t) \rangle$  (dark blue) and time-averaged survival probability  $\overline{\langle S_P(t) \rangle}$  (dark red) for the Rosenzweig-Porter model. The power-law decays  $\propto t^{-\gamma}$  and  $\propto t^{-\nu}$  are indicated with green dashed lines and the values of  $\gamma$  and  $\nu$  are shown in each panel. The time intervals chosen for the fittings are the same for both exponents. The values of the control parameter  $\alpha$  are also indicated;  $N = 12000$ .

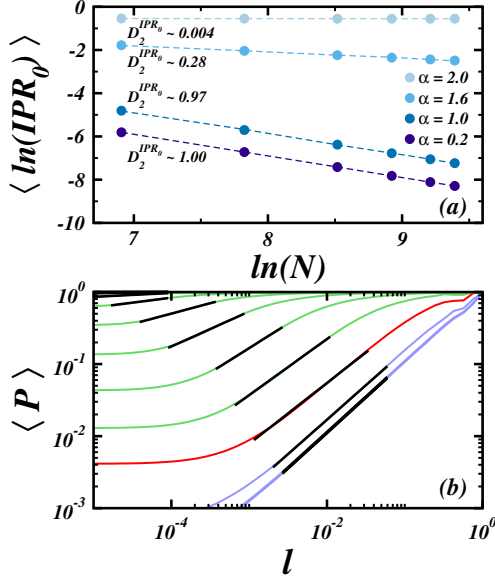


FIG. 3. (a) Scaling analysis of  $\langle \ln(\text{IPR}_0) \rangle$  to extract  $D_2^{\text{IPR}_0}$  and (b) scaling analysis of  $\langle P(l) \rangle$  from Eq. (8) to obtain  $D_2^{\text{box}}$  for the Rosenzweig-Porter model. The values of  $\alpha$  are indicated in (a). In (b), the blue lines are for  $\alpha < 1$ , the red curve corresponds to  $\alpha = 1$ , the green lines are for  $1 < \alpha$ , and the black lines are fitting curves;  $N = 12000$ .

phase. The exponent  $\gamma$ , associated with the survival probability, deviates from all three quantities throughout the delocalized and intermediate regimes, only approaching agreement in the localized phase ( $\alpha > 2$ ). In the delocalized phase,  $\gamma > 1$  and it approaches  $\gamma = 3$  for  $\alpha \rightarrow 0$ , as in the GOE model.

It is interesting that the four quantities distinguish the three regions:  $\alpha < 1$ ,  $1 < \alpha < 2$ , and  $\alpha > 2$ . They decay as  $\alpha$  increases in the nonergodic extended phase and are

nearly constant in the ergodic and localized regimes.

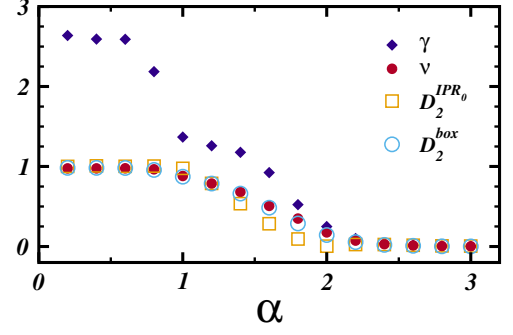


FIG. 4. Power-law exponents  $\gamma$  and  $\nu$ , and fractal dimensions  $D_2^{\text{IPR}_0}$  and  $D_2^{\text{box}}$  as a function of the control parameter  $\alpha$  for the Rosenzweig-Porter model.

### C. Power-law banded matrices

The PBRM model corresponds to an ensemble of real and symmetric  $N \times N$  matrices filled with real Gaussian random numbers whose mean is zero and the variance of its elements is given by

$$\langle H_{ij}^2 \rangle = \begin{cases} 1, & i = j \\ \left[ 1 + |(i-j)/\beta|^{2\alpha} \right]^{-1}, & i \neq j, \end{cases} \quad (17)$$

where  $\beta$  is the bandwidth and the control parameter  $\alpha$  can be varied from the delocalized phase ( $\alpha < 1$ ) to the localized phase ( $\alpha > 1$ ), with  $\alpha = 1$  being the critical point [13, 32, 33, 42, 75, 77]. We recover the GOE matrix when  $\alpha \rightarrow 0$  and the tight-binding model with nearest-neighbor random coupling (tridiagonal matrix) when  $\alpha \rightarrow \infty$ . Physically, the PBRM model can be interpreted as describing a particle in a one-dimensional disordered system with long-range hopping that decays as a power law [12, 75, 96].

The figures used to extract  $\gamma$ ,  $\nu$ ,  $D_2^{\text{IPR}_0}$ , and  $D_2^{\text{box}}$  are provided in the Appendix B. In Fig. 5(a), we compare the behavior of these four quantities as a function of the control parameter  $\alpha$  for fixed  $\beta = 1$ . The results are similar to those for the RP model, in the sense that there is excellent agreement between  $\nu$  and  $D_2^{\text{box}}$ , and reasonable agreement also with  $D_2^{\text{IPR}_0}$ , for any value of  $\alpha$ , while  $\gamma$  only approaches  $\nu$  in the localized regime ( $\alpha > 1$ ). In the delocalized region,  $\gamma$  decays abruptly as  $\alpha$  increases.

The largest fluctuations in the structures of the eigenstates happen at critical points, where the eigenstates are multifractal. This motivates the analysis in Fig. 5(b), where we fix  $\alpha = 1$  and compare the behavior of the four quantities,  $\gamma$ ,  $\nu$ ,  $D_2^{\text{IPR}_0}$ , and  $D_2^{\text{box}}$ , as a function of the bandwidth  $\beta$ . By increasing  $\beta$ , we can modify the degree of multifractality of the states, going from strong multifractality ( $\beta \ll 1$ ) to weak multifractality ( $\beta \gg 1$ ). As before, we find excellent agreement between  $\nu$  and

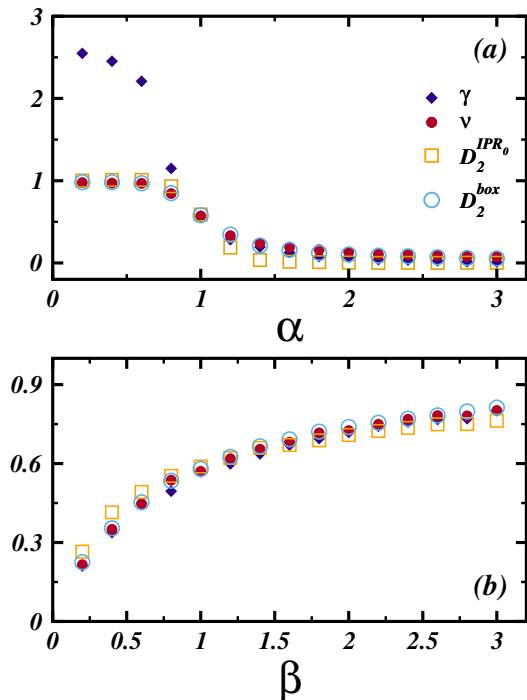


FIG. 5. Study of fractality for the power-law banded random matrix model. Power-law exponents  $\gamma$  and  $\nu$ , obtained for  $N = 12000$ , and fractal dimensions  $D_2^{\text{IPR}_0}$  and  $D_2^{\text{box}}$  as a function of (a) the control parameter  $\alpha$  for fixed  $\beta = 1$  and (b) the bandwidth  $\beta$  for the critical point  $\alpha = 1$ .

$D_2^{\text{box}}$ , and good agreement with  $D_2^{\text{IPR}_0}$ . Interestingly, the power-law exponent  $\gamma$  is also very similar to  $\nu$ , indicating that at the critical point, the power-law decay of  $\langle S_P(t) \rangle$  and  $\langle S_P(t) \rangle$  are comparable, as indeed seen in Fig. 9 provided in the Appendix B.

#### IV. INTERACTING MANY-BODY QUANTUM MODELS

The spin-1/2 Hamiltonian for the two one-dimensional (1D) physical models with nearest-neighbor couplings that we consider is given by

$$H = \frac{J}{4} \sum_{k=1}^{L-1} [\sigma_k^x \sigma_{k+1}^x + \sigma_k^y \sigma_{k+1}^y + \sigma_k^z \sigma_{k+1}^z] + \frac{1}{2} \sum_{k=1}^L h_k \sigma_k^z, \quad (18)$$

where  $\sigma_k^{x,y,z}$  are Pauli matrices that act on the particle at site  $k$ , the coupling strength is set to  $J = 1$ , and  $h_k$  corresponds to Zeeman splittings. The two models differ by the kind of onsite disorder that is chosen.

- We have the interacting Aubry-André model when  $h_k = h \cos(2\pi\beta k + \phi)$ , where  $\beta = (1 + \sqrt{2})/2$  is the inverse golden ratio,  $\phi$  is a random phase between 0 and  $2\pi$ , and  $h$  is the amplitude of the disorder strength. This model transitions from a delocalized phase when  $h < 0.7$  to a localized regime when  $h > 1.7$ , with an extended

nonergodic phase existing for  $0.7 < h < 1.7$  [106, 107].

- We have the disordered spin-1/2 Heisenberg model, when  $h_k$  are uncorrelated random numbers taken from a flat distribution with  $[-h, h]$  and  $h$  being the disorder strength. For  $h = 0$ , the model is integrable. As  $h$  increases from zero, the system becomes chaotic. Several numerical studies indicate that this transition should occur for an infinitesimally small value of  $h$  as  $L \rightarrow \infty$ . As the disorder is further increased, beyond the coupling strength, some studies suggest that the model transitions from a delocalized phase to a many-body localized regime, although there is no consensus on whether this holds [85, 108–111].

We construct the Hamiltonian matrix for both models in the largest subspace of the Hilbert space for which the total  $z$ -magnetization  $\frac{1}{2} \sum_{k=1}^L \sigma_k^z = 0$  and the dimension  $N = L!/((L/2)!)^2$ . The figures used to extract  $\gamma$ ,  $\nu$ ,  $D_2^{\text{IPR}_0}$ , and  $D_2^{\text{box}}$  for both models are provided in the appendix. Below, we compare the results as a function of the potential strength  $h$ .

##### A. Interacting Aubry-André model

Figure 6, obtained for the interacting Aubry-André model, shows excellent agreement between the power-law decay exponent  $\nu$  of  $\langle S_P(t) \rangle$  and the fractal dimension  $D_2^{\text{box}}$ , supporting our claim that these two quantities coincide in interacting many-body quantum systems. We also observe that in the intermediate regime ( $0.7 < h < 1.7$ ), the fractal dimension  $D_2^{\text{IPR}_0}$  now deviates more from  $\nu$  and  $D_2^{\text{box}}$  than what was seen for the RP and PBRM models. Even though  $D_2^{\text{box}}$  and  $D_2^{\text{IPR}_0}$  are both derived from the components  $C_n^{(0)}$  of the initial state, they rely on different approaches:  $D_2^{\text{IPR}_0}$  is based solely on the sum of  $|C_n^{(0)}|^4$ , while the box-counting method involves sums of components in windows of energies. The intermediate phase of the Aubry-André model makes the difference between these two constructions more evident. Furthermore, the faster decay of  $D_2^{\text{box}}$  and  $\nu$  with increasing  $h$  emphasizes their stronger sensitivity to multifractality compared to  $D_2^{\text{IPR}_0}$ .

The results for  $\gamma$  in Fig. 6 show that apart from the ergodic region, there is very good agreement with  $\nu$  for  $h > 0.7$ , that is, in the intermediate and localized regions. Deep in the chaotic region,  $\gamma$  is expected to get close to 2, consistent with the bounds of the energy distribution of the initial state [89, 90], which for physical many-body quantum systems is Gaussian. Deviations from  $\gamma = 2$  are caused by finite-size effects [112]. As  $h$  increases and the system approaches the intermediate region,  $\gamma$  decays abruptly. In the localized region, all four quantities are very close to zero.



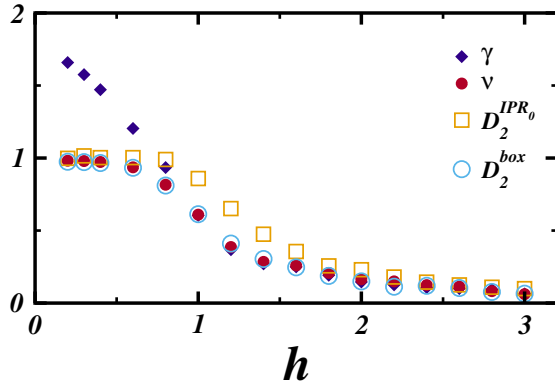


FIG. 6. Power-law exponents  $\gamma$  and  $\nu$  and fractal dimensions  $D_2^{\text{IPR}_0}$  and  $D_2^{\text{box}}$  as a function of the potential strength  $h$  for the interacting Aubry-André model with largest system size  $L = 16$  ( $N = 12870$ ).

### B. Disordered spin-1/2 Heisenberg model

Figure 7 shows  $\gamma$ ,  $\nu$ ,  $D_2^{\text{IPR}_0}$ , and  $D_2^{\text{box}}$  as a function of the disorder strength  $h$  for the Heisenberg model. Once again we confirm that  $\nu \approx D_2^{\text{box}}$  for interacting many-body quantum systems. The figures also reiterates that, similarly to the Aubry-André model,  $\gamma \rightarrow 2$  deep in the chaotic region, decaying as the disorder increases. Furthermore, as before,  $\nu$  and  $D_2^{\text{box}}$  decay faster than  $D_2^{\text{IPR}_0}$  as  $h$  increases above the coupling strength.

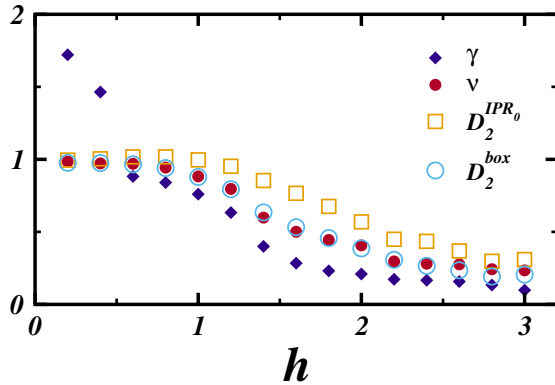


FIG. 7. Power-law exponents  $\gamma$  and  $\nu$  and fractal dimensions  $D_2^{\text{IPR}_0}$  and  $D_2^{\text{box}}$  as a function of the potential strength  $h$  for the spin-1/2 Heisenberg model with largest system size  $L = 16$  ( $N = 12870$ ).

Contrary to the Aubry-André model,  $\gamma$  in Fig. 7 deviates from  $\nu$  for all values of the disorder strength that are shown for  $h > J$ . At large disorder strengths, all four quantities,  $\nu$ ,  $D_2^{\text{box}}$ ,  $D_2^{\text{IPR}_0}$ , and  $\gamma$  exhibit fluctuations rather than a monotonic decay to zero. This behavior reflects the ongoing uncertainty surrounding the existence of a true many-body localized phase for this model.

## V. CONCLUSIONS

This work establishes the time-averaged survival probability as a powerful and practical tool for extracting the fractal dimension  $D_2$  in many-body quantum systems. Contrary to conventional methods that require finite-size scaling analysis of measures of delocalization, such as the inverse participation ratio, our approach resorts to dynamics to directly probe the structure of the states.

Using ensembles of Gaussian orthogonal, Rosenzweig-Porter, and power-law banded random matrices, and interacting many-body quantum systems described by the Aubry-André and disordered Heisenberg models, we demonstrated that the exponent  $\nu$  of the power-law decay of the time-averaged survival probability consistently coincides with the fractal dimension  $D_2^{\text{box}}$  evaluated using the box-counting method. The agreement between the two quantities,  $\nu \approx D_2^{\text{box}}$ , holds even in regimes where the survival probability decay exponent  $\gamma$  or fractal dimensions computed from inverse participation ratios (e.g.  $D_2^{\text{IPR}_0}$ ) fail to match among them and with  $\nu$ . This happens, for example, deep in the chaotic regime, where  $\gamma$  is larger than  $\nu$ , and in extended nonergodic phases, where  $D_2^{\text{IPR}_0}$  is usually larger than  $\nu$ .

In short, the time-averaged survival probability offers a robust and scalable approach to identifying extended nonergodic phases and multifractal behavior in complex quantum systems. It is a promising method for numerical studies, where the direct analysis of the structure of the states is restricted to small system sizes, and for experimental platforms, as it avoids state tomography.

## VI. ACKNOWLEDGMENTS

D. A. Z.-H. and E. J. T.-H. are grateful to Secihti México for financial support under project No. CF-2023-I-1748 and to VIEP-BUAP under project No. 100524481-VIEP2024. I.V.-F. and L.F.S. thank start-up funding from the University of Connecticut.

### Appendix A: Derivation of the time-averaged survival probability for GOE random matrices

The time-averaged survival probability is defined as

$$\overline{\langle S_P(t) \rangle} = \frac{1}{t} \int_0^t \langle S_P(t') \rangle dt' \quad (\text{A1})$$

For the GOE,

$$\langle S_P(t) \rangle = \frac{4}{3} \overline{S_P} N \frac{\mathcal{J}_1^2(2\Gamma t)}{(2\Gamma t)^2} - \frac{1}{3} \overline{S_P} b_2 \left( \frac{\Gamma t}{2N} \right) + \overline{S_P}, \quad (\text{A2})$$

where  $\Gamma = \sqrt{N/2}$ , and

$$b_2(t) = f(t)\Theta(1-t) + g(t)\Theta(t-1), \quad (\text{A3})$$

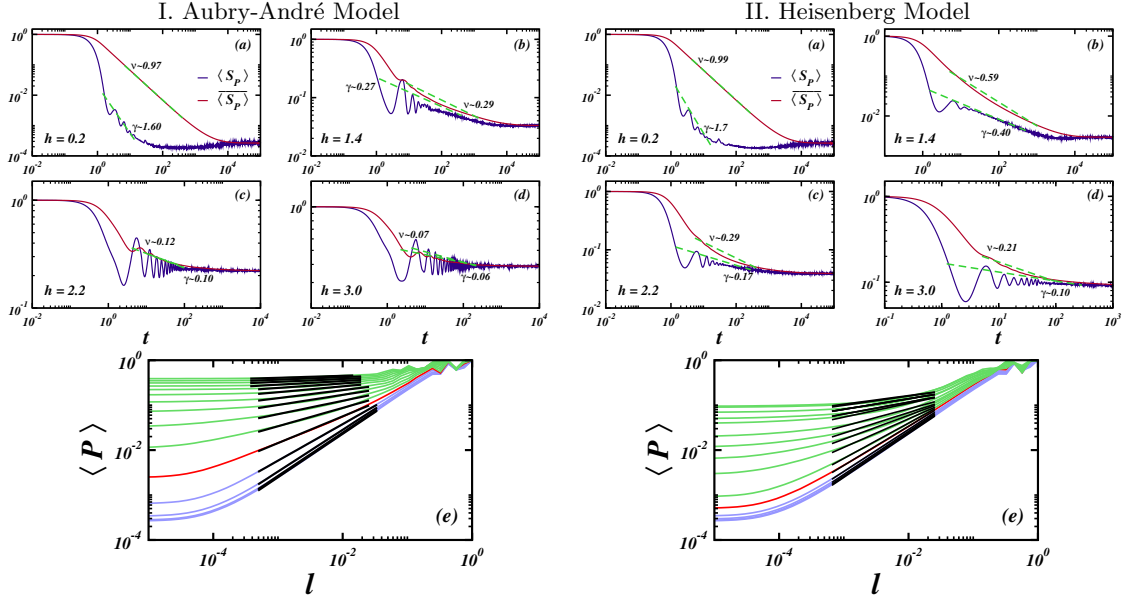


FIG. 8. Interacting Aubry-André model (left panels) and disordered Heisenberg model (right panels) for  $L = 16$  ( $N = 12870$ ). (a)-(d): Survival probability  $\langle S_P(t) \rangle$  (dark blue) and time-averaged survival probability  $\overline{\langle S_P(t) \rangle}$  (dark red). The power-law decays  $\propto t^{-\gamma}$  and  $\propto t^{-\nu}$  are indicated with green dashed lines and the values of  $\gamma$  and  $\nu$  are shown in each panel. The time intervals chosen for the fittings are the same for both exponents. The values of the disordered strength  $h$  are also indicated. (e): Scaling analysis of  $\langle P(l) \rangle$  from Eq. (8) to obtain  $D_2^{\text{box}}$ . The blue lines are for  $h < 1$ , the red curve corresponds to  $h = 1$ , the green lines are for  $h > 1$ , and the black lines are fitting curves.

with

$$f(t) = 1 - 2t + t \ln(2t + 1),$$

$$g(t) = t \ln \left( \frac{2t + 1}{2t - 1} \right) - 1.$$

Then,

$$\overline{\langle S_P(t) \rangle} = \frac{4}{3} \overline{S_P} N \mathcal{I}_1(u) - \frac{1}{3} \overline{S_P} \mathcal{I}_2(v) + \overline{S_P}, \quad (\text{A4})$$

where  $u = 2\Gamma t$ ,  $v = \Gamma t/2N$ ,

$$\mathcal{I}_1(u) = \frac{1}{u} \int_0^u \frac{\mathcal{J}_1^2(x)}{x^2} dx$$

$$= \frac{2 [\mathcal{J}_0^2(u) + \mathcal{J}_1^2(u)]}{3} - \frac{2 \mathcal{J}_0(u) \mathcal{J}_1(u)}{3u} - \frac{\mathcal{J}_1^2(u)}{3u^2}, \quad (\text{A5})$$

and

$$\mathcal{I}_2(v) = \frac{1}{v} \int_0^v b_2(x) dx = F(v) \Theta(1 - v) + G(v) \Theta(v - 1), \quad (\text{A6})$$

where

$$F(v) = \frac{5}{4}(1 - v) + \left( \frac{v}{2} - \frac{1}{8v} \right) \ln(1 + 2v),$$

$$G(v) = \frac{1}{2v}(1 - v) + \left( \frac{v}{2} - \frac{1}{8v} \right) \ln \left( 1 + \frac{2}{2v - 1} \right).$$

To obtain an expression for the asymptotic behavior of  $\overline{\langle S_P(t) \rangle}$  in Eq. (15), we evaluate  $\mathcal{I}_1(u \rightarrow \infty)$  and  $\mathcal{I}_2(v \rightarrow \infty)$  given in Eqs. (13)-(14).

## Appendix B: Additional results for power-law banded random matrices and spin-1/2 models

Here, we provide representative figures that illustrate how (i) the power-law exponent  $\gamma$  is obtained from the analysis of the decay of the survival probability,  $\langle S_P(t) \rangle \propto t^{-\gamma}$ , (ii) the power-law exponent  $\nu$  is obtained from the analysis of the decay of the time-averaged survival probability,  $\overline{\langle S_P(t) \rangle} \propto t^{-\nu}$ , and (iii) the fractal dimension  $D_2^{\text{box}}$  is extracted from the scaling analysis of  $\langle P(l) \rangle$ . These results are shown in Fig. 8 for the interacting physical spin models and in Fig. 9 for the PBRM model.

The left and right panels displayed in Figs. 8(a)-(d) show the evolution of the survival probability  $\langle S_P(t) \rangle$  and of the time-averaged survival probability  $\overline{\langle S_P(t) \rangle}$  for the interacting Aubry-André model (left panels) and the disordered Heisenberg model (right panels). Both models exhibit power-law decays for both quantities at intermediate times. The bottom left and right Fig. 8(d) show the analysis of  $\langle P(l) \rangle$  from Eq. (8). The slope of the black curves for  $\langle P(l) \rangle$  decreases as the disorder strength  $h$  increases, resulting in smaller values of  $D_2^{\text{box}}$  as one moves away from the chaotic region.

Figure 9 shows the evolution of the survival probability  $\langle S_P(t) \rangle$  and of the time-averaged survival probability  $\overline{\langle S_P(t) \rangle}$  for PBRM matrices at the critical point  $\alpha = 1$  and for different values of the bandwidth  $\beta$ . Contrary to the chaotic region, where  $\langle S_P(t) \rangle$  for the PBRM model shows oscillations during its power-law decay as in Fig. 1



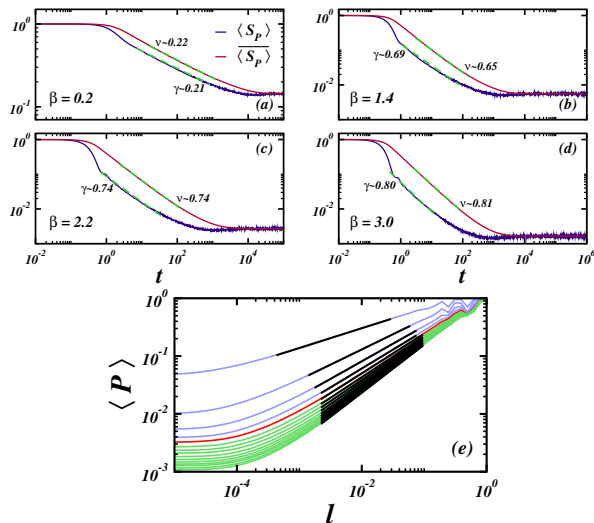


FIG. 9. Power-law banded random matrix model at the critical point  $\alpha = 1$  and  $N = 12000$ . (a)-(d): Survival probability  $\langle S_P(t) \rangle$  (dark blue) and time-averaged survival probability  $\overline{\langle S_P(t) \rangle}$  (dark red). The power-law decays  $\propto t^{-\gamma}$  and  $\propto t^{-\nu}$  are indicated with green dashed lines and the values of  $\gamma$  and  $\nu$  are shown in each panel. The time intervals chosen for the fittings are the same for both exponents. The values of the bandwidth  $\beta$  are also indicated. (e): Scaling analysis of  $\langle P(l) \rangle$  from Eq. (8) to obtain  $D_2^{\text{box}}$ . The blue lines are for  $\beta < 1$ , the red curve corresponds to  $\beta = 1$ , the green lines are for  $\beta > 1$ , and the black lines are fitting curves.

of the GOE model, at the critical point,  $\langle S_P(t) \rangle$  decays smoothly and similarly to  $\overline{\langle S_P(t) \rangle}$ . Indeed, we can see in Figs. 9(a)-(d) that the decay rates for both quantities coincide, that is,  $\gamma \sim \nu$ .

Figure 9(e) shows the analysis of  $\langle P(l) \rangle$  from Eq. (8) for the PBRM model at the critical point  $\alpha = 1$  for different values of the bandwidth  $\beta$ . To extract the fractal dimension, we concentrate on the region indicated with black lines. The slope is larger and  $D_2^{\text{box}}$  is closer to 1 for larger  $\beta$ .

- 
- [1] F. Wegner, Inverse participation ratio in  $2 + \epsilon$  dimensions, Z. Phys. B **36**, 209 (1980).
  - [2] C. M. Soukoulis and E. N. Economou, Fractal character of eigenstates in disordered systems, Phys. Rev. Lett. **52**, 565 (1984).
  - [3] C. Castellani and L. Peliti, Multifractal wavefunction at the localisation threshold, J. Phys. A **19**, L429 (1986).
  - [4] R. Ketzmerick, G. Petschel, and T. Geisel, Slow decay of temporal correlations in quantum systems with cantor spectra, Phys. Rev. Lett. **69**, 695 (1992).
  - [5] B. Huckestein and L. Schweitzer, Relation between the correlation dimensions of multifractal wave functions and spectral measures in integer quantum Hall systems, Phys. Rev. Lett. **72**, 713 (1994).
  - [6] J. X. Zhong and R. Mosseri, Quantum dynamics in quasiperiodic systems, Journal of Physics: Condensed Matter **7**, 8383 (1995).
  - [7] H. Q. Yuan, U. Grimm, P. Repetowicz, and M. Schreiber, Energy spectra, wave functions, and quantum diffusion for quasiperiodic systems, Phys. Rev. B **62**, 15569 (2000).
  - [8] B. Huckestein, Scaling theory of the integer quantum hall effect, Rev. Mod. Phys. **67**, 357 (1995).
  - [9] B. Huckestein and R. Klesse, Spatial and spectral multifractality of the local density of states at the mobility edge, Phys. Rev. B **55**, R7303 (1997).
  - [10] B. Huckestein and R. Klesse, Wave-packet dynamics at the mobility edge in two- and three-dimensional systems, Phys. Rev. B **59**, 9714 (1999).
  - [11] M. Schreiber and H. Grussbach, Multifractal wave functions at the Anderson transition, Phys. Rev. Lett. **67**, 607 (1991).
  - [12] F. Evers and A. D. Mirlin, Fluctuations of the inverse participation ratio at the Anderson transition, Phys. Rev. Lett. **84**, 3690 (2000).
  - [13] F. Evers and A. D. Mirlin, Anderson transitions, Rev. Mod. Phys. **80**, 1355 (2008).
  - [14] C. Yang, Y. Wang, P. Wang, X. Gao, and S. Chen, Dynamical signature of localization-delocalization transition in a one-dimensional incommensurate lattice, Phys. Rev. B **95**, 184201 (2017).
  - [15] V. K. Varma, C. de Mulatier, and M. Žnidarič, Fractality in nonequilibrium steady states of quasiperiodic systems, Phys. Rev. E **96**, 032130 (2017).
  - [16] X. Deng, S. Ray, S. Sinha, G. V. Shlyapnikov, and L. Santos, One-dimensional quasicrystals with power-law hopping, Phys. Rev. Lett. **123**, 025301 (2019).
  - [17] Z. Xu, H. Huangfu, Y. Zhang, and S. Chen, Dynamical observation of mobility edges in one-dimensional incommensurate optical lattices, New J. Phys. **22**, 013036 (2020).
  - [18] A. Jagannathan, The fibonacci quasicrystal: Case study of hidden dimensions and multifractality, Rev. Mod. Phys. **93**, 045001 (2021).
  - [19] E. J. Torres-Herrera and L. F. Santos, Dynamics at the many-body localization transition, Phys. Rev. B **92**,

- 014208 (2015).
- [20] D. J. Luitz, N. Laflorencie, and F. Alet, Extended slow dynamical regime close to the many-body localization transition, *Phys. Rev. B* **93**, 060201 (2016).
  - [21] M. Schiulaz, E. J. Torres-Herrera, and L. F. Santos, Thouless and relaxation time scales in many-body quantum systems, *Phys. Rev. B* **99**, 174313 (2019).
  - [22] N. Laflorencie, G. Lemarié, and N. Macé, Chain breaking and Kosterlitz-Thouless scaling at the many-body localization transition in the random-field Heisenberg spin chain, *Phys. Rev. Res.* **2**, 042033 (2020).
  - [23] A. Solórzano, L. F. Santos, and E. J. Torres-Herrera, Multifractality and self-averaging at the many-body localization transition, *Phys. Rev. Research* **3**, L032030 (2021).
  - [24] Q. Wang and M. Robnik, Multifractality in quasienergy space of coherent states as a signature of quantum chaos, *Entropy* **23**, 10.3390/e23101347 (2021).
  - [25] M. Sarkar, R. Ghosh, A. Sen, and K. Sengupta, Signatures of multifractality in a periodically driven interacting Aubry-André model, *Phys. Rev. B* **105**, 024301 (2022).
  - [26] P. Sierant and X. Turkeshi, Universal behavior beyond multifractality of wave functions at measurement-induced phase transitions, *Phys. Rev. Lett.* **128**, 130605 (2022).
  - [27] M. A. Bastarrachea-Magnani, D. Villaseñor, J. Chávez-Carlos, S. Lerma-Hernández, L. F. Santos, and J. G. Hirsch, Quantum multifractality as a probe of phase space in the Dicke model, *Phys. Rev. E* **109**, 034202 (2024).
  - [28] D. S. Bhakuni and Y. B. Lev, Dynamic scaling relation in quantum many-body systems, *Phys. Rev. B* **110**, 014203 (2024).
  - [29] P. Sierant, M. Lewenstein, A. Scardicchio, L. Vidmar, and J. Zakrzewski, Many-body localization in the age of classical computing\*, *Rep. Progr. Phys.* **88**, 026502 (2025).
  - [30] A. K. Das, A. Ghosh, and I. M. Khaymovich, Emergent multifractality in power-law decaying eigenstates (2025), [arXiv:2501.17242](https://arxiv.org/abs/2501.17242) [cond-mat.dis-nn].
  - [31] S. Hamanaka and K. Kawabata, Multifractality of the many-body non-Hermitian skin effect, *Phys. Rev. B* **111**, 035144 (2025).
  - [32] I. Varga and D. Braun, Critical statistics in a power-law random-banded matrix ensemble, *Phys. Rev. B* **61**, R11859 (2000).
  - [33] A. D. Mirlin, Statistics of energy levels and eigenfunctions in disordered systems, *Phys. Rep.* **326**, 259 (2000).
  - [34] I. Varga, Fluctuation of correlation dimension and inverse participation number at the Anderson transition, *Phys. Rev. B* **66**, 094201 (2002).
  - [35] E. Bogomolny and O. Giraud, Eigenfunction entropy and spectral compressibility for critical random matrix ensembles, *Phys. Rev. Lett.* **106**, 044101 (2011).
  - [36] J. A. Méndez-Bermúdez, A. Alcázar-López, and I. Varga, Multifractal dimensions for critical random matrix ensembles, *Europhys. Lett.* **98**, 37006 (2012).
  - [37] N. Laflorencie, Quantum entanglement in condensed matter systems, *Phys. Rep.* **646**, 1 (2016).
  - [38] A. Bäcker, M. Haque, and I. M. Khaymovich, Multifractal dimensions for random matrices, chaotic quantum maps, and many-body systems, *Phys. Rev. E* **100**, 032117 (2019).
  - [39] M. Carrera-Núñez, A. Martínez-Argüello, and J. Méndez-Bermúdez, Multifractal dimensions and statistical properties of critical ensembles characterized by the three classical wigner-dyson symmetry classes, *Physica A* **573**, 125965 (2021).
  - [40] W. Chen, O. Giraud, J. Gong, and G. Lemarié, Describing the critical behavior of the Anderson transition in infinite dimension by random-matrix ensembles: Logarithmic multifractality and critical localization, *Phys. Rev. B* **110**, 014210 (2024).
  - [41] W. Buijsman, M. Haque, and I. M. Khaymovich, Power-law banded random matrix ensemble as a model for quantum many-body Hamiltonians (2025), [arXiv:2503.08825](https://arxiv.org/abs/2503.08825) [cond-mat.dis-nn].
  - [42] V. E. Kravtsov and K. A. Muttalib, New class of random matrix ensembles with multifractal eigenvectors, *Phys. Rev. Lett.* **79**, 1913 (1997).
  - [43] V. Kravtsov, Critical spectral statistics as the luttinger liquid of energy levels at a finite temperature, *Annalen der Physik* **511**, 621 (1999).
  - [44] V. E. Kravtsov and A. M. Tsvelik, Energy level dynamics in systems with weakly multifractal eigenstates: Equivalence to one-dimensional correlated fermions at low temperatures, *Phys. Rev. B* **62**, 9888 (2000).
  - [45] M. L. Ndawana and V. E. Kravtsov, Energy level statistics of a critical random matrix ensemble, *Journal of Physics A: Mathematical and General* **36**, 3639 (2003).
  - [46] C. Monthus, Many-body-localization transition in the strong disorder limit: Entanglement entropy from the statistics of rare extensive resonances, *Entropy* **18**, 122 (2016).
  - [47] C. Monthus, Multifractality of eigenstates in the delocalized non-ergodic phase of some random matrix models: Wigner-weisskopf approach, *Journal of Physics A: Mathematical and Theoretical* **50**, 295101 (2017).
  - [48] P. Sierant, M. Schirò, M. Lewenstein, and X. Turkeshi, Measurement-induced phase transitions in  $(d + 1)$ -dimensional stabilizer circuits, *Phys. Rev. B* **106**, 214316 (2022).
  - [49] X. Turkeshi, M. Schirò, and P. Sierant, Measuring non-stabilizerness via multifractal flatness, *Phys. Rev. A* **108**, 042408 (2023).
  - [50] R. Yousefjani and A. Bayat, Mobility edge in long-range interacting many-body localized systems, *Phys. Rev. B* **107**, 045108 (2023).
  - [51] M. Hopjan and L. Vidmar, Scale-invariant survival probability at eigenstate transitions, *Phys. Rev. Lett.* **131**, 060404 (2023).
  - [52] F. M. Izrailev, Simple models of quantum chaos: Spectrum and eigenfunctions, *Phys. Rep.* **196**, 299 (1990).
  - [53] C. R. de Oliveira and G. Q. Pellegrino, Quantum return probability for substitution potentials, *Journal of Physics A: Mathematical and General* **32**, L285 (1999).
  - [54] S. N. Evangelou and D. E. Katsanos, Multifractal quantum evolution at a mobility edge, *Journal of Physics A: Mathematical and General* **26**, L1243 (1993).
  - [55] T. Kawarabayashi and T. Ohtsuki, Diffusion of electrons in two-dimensional disordered symplectic systems, *Phys. Rev. B* **53**, 6975 (1996).
  - [56] C. Karrasch, J. Hauschild, S. Langer, and F. Heidrich-Meisner, Drude weight of the spin- $\frac{1}{2}$  XXZ chain: Density matrix renormalization group versus exact diagonalization, *Phys. Rev. B* **87**, 245128 (2013).
  - [57] T. Chanda, P. Sierant, and J. Zakrzewski, Time dynam-

- ics with matrix product states: Many-body localization transition of large systems revisited, *Phys. Rev. B* **101**, 035148 (2020).
- [58] A. Strathearn, P. Kirton, D. Kilda, J. Keeling, and B. W. Lovett, Efficient non-markovian quantum dynamics using time-evolving matrix product operators, *Nat. Commun.* **9**, 3322 (2018).
- [59] Z. Hu, R. Xia, and S. Kais, A quantum algorithm for evolving open quantum dynamics on quantum computing devices, *Sci. Rep.* **10**, 3301 (2020).
- [60] M. C. Bañuls, N. Y. Yao, S. Choi, M. D. Lukin, and J. I. Cirac, Dynamics of quantum information in many-body localized systems, *Phys. Rev. B* **96**, 174201 (2017).
- [61] E. J. Torres-Herrera, M. Távara, and L. F. Santos, Survival probability of the Néel state in clean and disordered systems: an overview, *Braz. J. Phys.* **46**, 239 (2015).
- [62] P. Grassberger and I. Procaccia, Estimation of the kolmogorov entropy from a chaotic signal, *Phys. Rev. A* **28**, 2591 (1983).
- [63] T. C. Halsey, M. H. Jensen, L. P. Kadanoff, I. Procaccia, and B. I. Shraiman, Fractal measures and their singularities: The characterization of strange sets, *Phys. Rev. A* **33**, 1141 (1986).
- [64] W. Pook and M. Janßen, Multifractality and scaling in disordered mesoscopic systems, *Zeitschrift für Physik B Condensed Matter* **82**, 295 (1991).
- [65] M. Janssen, Multifractal analysis of broadly-distributed observables at criticality, *International Journal of Modern Physics B* **08**, 943 (1994).
- [66] D. A. Zarate-Herrada, L. F. Santos, and E. J. Torres-Herrera, Generalized survival probability, *Entropy* **25**, 205 (2023).
- [67] L. F. Santos and E. J. Torres-Herrera, Analytical expressions for the evolution of many-body quantum systems quenched far from equilibrium, *AIP Conference Proceedings* **1912**, 020015 (2017).
- [68] E. J. Torres-Herrera, A. M. García-García, and L. F. Santos, Generic dynamical features of quenched interacting quantum systems: Survival probability, density imbalance, and out-of-time-ordered correlator, *Phys. Rev. B* **97**, 060303 (2018).
- [69] M. L. Mehta, *Random Matrices* (Academic Press, Boston, 1991).
- [70] N. Rosenzweig and C. E. Porter, "repulsion of energy levels" in complex atomic spectra, *Phys. Rev.* **120**, 1698 (1960).
- [71] I. M. Khaymovich and V. E. Kravtsov, Dynamical phases in a "multifractal" Rosenzweig-Porter model, *SciPost Phys.* **11**, 045 (2021).
- [72] D. Venturelli, L. F. Cugliandolo, G. Schehr, and M. Tarzia, Replica approach to the generalized Rosenzweig-Porter model, *SciPost Phys.* **14**, 110 (2023).
- [73] X. Zhang, W. Zhang, J. Che, and B. Dietz, Experimental test of the rosenzweig-porter model for the transition from poisson to gaussian unitary ensemble statistics, *Phys. Rev. E* **108**, 044211 (2023).
- [74] W. Buijsman, Long-range spectral statistics of the rosenzweig-porter model, *Phys. Rev. B* **109**, 024205 (2024).
- [75] A. D. Mirlin, Y. V. Fyodorov, F.-M. Dittes, J. Quezada, and T. H. Seligman, Transition from localized to extended eigenstates in the ensemble of power-law random banded matrices, *Phys. Rev. E* **54**, 3221 (1996).
- [76] E. Bogomolny and M. Sieber, Power-law random banded matrices and ultrametric matrices: Eigenvector distribution in the intermediate regime, *Phys. Rev. E* **98**, 042116 (2018).
- [77] W.-J. Rao, Power-law random banded matrix ensemble as the effective model for many-body localization transition, *The European Physical Journal Plus* **137**, 398 (2022).
- [78] G. De Tomasi and I. M. Khaymovich, Non-hermiticity induces localization: Good and bad resonances in power-law random banded matrices, *Phys. Rev. B* **108**, L180202 (2023).
- [79] J. A. Méndez-Bermúdez, A. Alcázar-López, and I. Varga, Multifractal dimensions for critical random matrix ensembles, *Europhys. Lett.* **98**, 37006 (2012).
- [80] G. De Tomasi and I. M. Khaymovich, Non-hermiticity induces localization: Good and bad resonances in power-law random banded matrices, *Phys. Rev. B* **108**, L180202 (2023).
- [81] S. Iyer, V. Oganesyan, G. Refael, and D. A. Huse, Many-body localization in a quasiperiodic system, *Phys. Rev. B* **87**, 134202 (2013).
- [82] M. Schreiber, S. S. Hodgman, P. Bordia, H. P. Lüschen, M. H. Fischer, R. Vosk, E. Altman, U. Schneider, and I. Bloch, Observation of many-body localization of interacting fermions in a quasirandom optical lattice, *Science* **349**, 842 (2015).
- [83] L. F. Santos, G. Rigolin, and C. O. Escobar, Entanglement versus chaos in disordered spin systems, *Phys. Rev. A* **69**, 042304 (2004).
- [84] L. F. Santos, Transport and control in one-dimensional systems, *J. Math. Phys.* **50**, 095211 (1 (2009).
- [85] J. Šuntajs, J. Bonča, T. c. v. Prosen, and L. Vidmar, Quantum chaos challenges many-body localization, *Phys. Rev. E* **102**, 062144 (2020).
- [86] E. J. Torres-Herrera, M. Vyas, and L. F. Santos, General features of the relaxation dynamics of interacting quantum systems, *New J. Phys.* **16**, 063010 (2014).
- [87] E. J. Torres-Herrera and L. F. Santos, Nonexponential fidelity decay in isolated interacting quantum systems, *Phys. Rev. A* **90**, 033623 (2014).
- [88] J. Chalker, Scaling and eigenfunction correlations near a mobility edge, *Physica A* **167**, 253 (1990).
- [89] M. Távara, E. J. Torres-Herrera, and L. F. Santos, Inevitable power-law behavior of isolated many-body quantum systems and how it anticipates thermalization, *Phys. Rev. A* **94**, 041603 (2016).
- [90] M. Távara, E. J. Torres-Herrera, and L. F. Santos, Power-law decay exponents: A dynamical criterion for predicting thermalization, *Phys. Rev. A* **95**, 013604 (2017).
- [91] E. J. Torres-Herrera and L. F. Santos, Extended nonergodic states in disordered many-body quantum systems, *Ann. Phys. (Berlin)* **529**, 1600284 (2017).
- [92] L. A. Khal'fin, Contribution to the decay theory of a quasi-stationary state, *Sov. Phys. JETP* **6**, 1053 (1958).
- [93] L. Fonda, G. C. Ghirardi, and A. Rimini, Decay theory of unstable quantum systems, *Rep. Prog. Phys.*, **41**, 587 (1978).
- [94] K. Urbanowski, General properties of the evolution of unstable states at long times, *Eur. Phys. J. D* **54**, 25 (2009).
- [95] J. Bauer, T.-M. Chang, and J. L. Skinner, Correlation length and inverse-participation-ratio exponents and

- multifractal structure for anderson localization, *Phys. Rev. B* **42**, 8121 (1990).
- [96] A. D. Mirlin and F. Evers, Multifractality and critical fluctuations at the Anderson transition, *Phys. Rev. B* **62**, 7920 (2000).
- [97] A. Mildenberger, F. Evers, and A. D. Mirlin, Dimensionality dependence of the wave-function statistics at the anderson transition, *Phys. Rev. B* **66**, 033109 (2002).
- [98] Y. Alhassid and R. D. Levine, Spectral autocorrelation function in the statistical theory of energy levels, *Phys. Rev. A* **46**, 4650 (1992).
- [99] E. J. Torres-Herrera, J. Karp, M. Távora, and L. F. Santos, Realistic many-body quantum systems vs. full random matrices: Static and dynamical properties, *Entropy* **18**, 359 (2016).
- [100] L. Leviandier, M. Lombardi, R. Jost, and J. P. Pique, Fourier transform: A tool to measure statistical level properties in very complex spectra, *Phys. Rev. Lett.* **56**, 2449 (1986).
- [101] E. J. Torres-Herrera and L. F. Santos, Dynamical manifestations of quantum chaos: correlation hole and bulge, *Philos. Trans. Royal Soc. A* **375**, 20160434 (2017).
- [102] A. K. Das, C. Cianci, D. G. A. Cabral, D. A. Zarate-Herrada, P. Pinney, S. Pilatowsky-Cameo, A. S. Matsoukas-Roubéas, V. S. Batista, A. del Campo, E. J. Torres-Herrera, and L. F. Santos, Proposal for many-body quantum chaos detection, *Phys. Rev. Res.* **7**, 013181 (2025).
- [103] M. Pino, J. Tabanera, and P. Serna, From ergodic to non-ergodic chaos in rosenzweig-porter model, *Journal of Physics A: Mathematical and Theoretical* **52**, 475101 (2019).
- [104] P. von Soosten and S. Warzel, Non-ergodic delocalization in the rosenzweig-porter model, *Lett. Math. Phys.* **109**, 905 (2019).
- [105] P. A. Nosov, I. M. Khaymovich, and V. E. Kravtsov, Correlation-induced localization, *Phys. Rev. B* **99**, 104203 (2019).
- [106] S. Xu, X. Li, Y.-T. Hsu, B. Swingle, and S. Das Sarma, Butterfly effect in interacting aubry-andre model: Thermalization, slow scrambling, and many-body localization, *Phys. Rev. Res.* **1**, 032039 (2019).
- [107] S. Xu, X. Li, Y.-T. Hsu, B. Swingle, and S. Das Sarma, Butterfly effect in interacting Aubry-André' model: Thermalization, slow scrambling, and many-body localization, *Phys. Rev. Res.* **1**, 032039 (2019).
- [108] D. J. Luitz, N. Laflorencie, and F. Alet, Many-body localization edge in the random-field Heisenberg chain, *Phys. Rev. B* **91**, 081103 (2015).
- [109] M. Serbyn, Z. Papić, and D. A. Abanin, Criterion for many-body localization-delocalization phase transition, *Phys. Rev. X* **5**, 041047 (2015).
- [110] J. Colbois, F. Alet, and N. Laflorencie, Statistics of systemwide correlations in the random-field xxz chain: Importance of rare events in the many-body localized phase, *Phys. Rev. B* **110**, 214210 (2024).
- [111] J. Niedda, G. B. Testasecca, G. Magnifico, F. Balducci, C. Vanoni, and A. Scardicchio, Renormalization-group analysis of the many-body localization transition in the random-field xxz chain (2024), arXiv:2410.12430 [cond-mat.dis-nn].
- [112] E. J. Torres-Herrera and L. F. Santos, Signatures of chaos and thermalization in the dynamics of many-body quantum systems, *Eur. Phys. J. Spec. Top.* **227**, 1897 (2019).